International Journal of Pharmaceutics 456 (2013) 269–281

Contents lists available at ScienceDirect

International Journal of Pharmaceutics

journal homepage: www.elsevier.com/locate/ijpharm

Pharmaceutical Nanotechnology

Dexamethasone-loaded poly(ε-caprolactone)/silica nanoparticles composites prepared by supercritical CO_2 foaming/mixing and deposition

M.B.C. de Matos[a], A.P. Piedade[b], C. Alvarez-Lorenzo[c], A. Concheiro[c], M.E.M. Braga[a,*], H.C. de Sousa[a,**]

[a] CIEPQPF, Chemical Engineering Department, FCTUC, University of Coimbra, Rua Sílvio Lima, Pólo II – Pinhal de Marrocos, 3030-790 Coimbra, Portugal
[b] CEMUC, Mechanical Engineering Department, FCTUC, University of Coimbra, Rua Luís Reis Santos, Pólo II – Pinhal de Marrocos, 3030-788 Coimbra, Portugal
[c] Departamento de Farmacia y Tecnología Farmacéutica, Facultad de Farmacia, Universidad de Santiago de Compostela, 15782 Santiago de Compostela, Spain

ARTICLE INFO

Article history:
Received 17 June 2013
Received in revised form 22 August 2013
Accepted 24 August 2013
Available online 2 September 2013

Keywords:
Poly(ε-caprolactone)
Mezoporous silica nanoparticles
Composites
Supercritical CO_2 foaming/mixing
Supercritical CO_2 impregnation/deposition

ABSTRACT

A supercritical carbon dioxide ($scCO_2$)-assisted foaming/mixing method (SFM) was implemented for preparing dexamethasone (DXMT)-loaded poly(ε-caprolactone)/silica nanoparticles (PCL/SNPs) composite materials suitable for bone regeneration. The composites were prepared from PCL and mesoporous SNPs (MCM-41/SBA-15) by means of $scCO_2$-assisted SFM at several operational pressures, processing times and depressurization conditions. DXMT was loaded into SNPs (applying a $scCO_2$ solvent impregnation/deposition method – SSID) and into PCL/SNPs composites (using the SFM method). The effects of the employed operational and compositional variables on the physicochemical and morphological features as well as in the in vitro release profiles of DXMT were analyzed in detail. This work demonstrates that the above-referred $scCO_2$-based methods can be very useful for the preparation of DXMT-loaded PCL/SNPs composites with tunable physicochemical, thermomechanical, morphological and drug release properties and suitable for hard-tissue regeneration applications.

1. Introduction

Tissue engineering (TE) involves the use of cells and biomaterials/scaffolds in order to repair, to regenerate or even to replace a lost function of a tissue and/or organ. Moreover and for the success of these approaches, scaffolds should also have the ability to carry and release (in a temporal- and in a 3D-controlled way) some specific biological and/or synthetic bioactive substances that are beneficial for the involved biological processes (Burg et al., 2000; Harrison, 2007; Tabata, 2005). TE scaffolds and their component biomaterials should satisfy a wide range of requirements, namely in terms of biocompatibility/toxicity, surface chemistry/morphology, porosity and pore morphology/interconnectivity, mechanical properties, degradation and bio-absorption rates and replacement rate of scaffolds by neo-tissues. Other relevant aspects include acceptable shelf-lives, as well as sterilization, processability and cost-effective industrial production. In addition, issues regarding drug loading capacity, distribution (homogeneous, heterogeneous, superficial or in discrete areas), release kinetics, binding affinity and stability of the drug should be satisfied (Harrison, 2007; Liu et al., 2008; Sachlos and Czernuszka, 2003; Salgado et al., 2004). The preparation of 3D scaffolds able to fulfill the above-referred requirements can be carried out applying several, well known techniques. Most of these methods make use of dangerous/toxic solvents/chemicals (that must be removed by additional extraction/purification steps) or of other harsh processing conditions (e.g. high temperature and extreme pH) that may promote the chemical/thermal degradation of the involved substances, namely of labile biopolymers, drugs, proteins or growth factors (Burg et al., 2000; Harrison, 2007; Liu et al., 2008; Reverchon and Cardea, 2012; Sachlos and Czernuszka, 2003; Salgado et al., 2004; Tai et al., 2007a).

Alternative methods based on supercritical fluids (SCFs), and namely on supercritical carbon dioxide ($scCO_2$), are known to be viable routes to overcome some of the above-mentioned problems. SCFs present unique (and tunable) properties that allow their application as solvents, anti-solvents or solutes in pharmaceutical and biomedical fields. $scCO_2$ has been widely employed to micronize bioactive substances and biocompatible polymers; to

* Corresponding author. Tel.: +351 239798758; fax: +351 239 798703.
** Corresponding author. Tel.: +351 239798749; fax: +351 239798703.
E-mail addresses: marabraga@eq.uc.pt (M.E.M. Braga), hsousa@eq.uc.pt, herminiosousa@gmail.com (H.C. de Sousa).

0378-5173/$ – see front matter © 2013 Elsevier B.V. All rights reserved.
http://dx.doi.org/10.1016/j.ijpharm.2013.08.042

prepare cyclodextrin-based drug-inclusion complexes; to encapsulate, impregnate or deposit bioactive substances into solid matrices (polymeric/ceramic/composite); and as a morphological, porogenic, foaming, viscosity reducer or a plasticizer agent in polymer/composite processing (Braga et al., 2011; Dash and Konkimalla, 2012; Elvassore and Kikic, 2001; Fleming and Kazarian, 2005; Jenkins et al., 2006; Kazarian, 2000; Kiran, 2009; Kikic and Vecchione, 2003; Banchero and Manna, 2012; Natu et al, 2008; Reverchon and Cardea, 2012; Shieh et al., 2009; Subramaniam et al., 1997; Tai et al., 2007a, 2007b; Xu et al., 2004).

In the particular case of polymeric or polymer/ceramic composite scaffolds for hard tissue applications, specific pore morphologies and incorporation/mixture of additives may be achieved by employing the so-called $scCO_2$-assisted foaming/mixing method (SFM). At certain pressure and temperature conditions, $scCO_2$ can be absorbed (as a solute) in relatively high amounts by amorphous and semi-crystalline polymers, leading to their plasticization and even to the formation of polymer melts (Davies et al., 2008; Fanovich and Jaeger, 2012; Howdle et al., 2001; Jenkins et al., 2006; Kiran et al., 2008; Kiran, 2009; Mooney et al., 1996; Tsivintzelis et al., 2007). Polymers in this liquid-like rubbery state may be homogeneous or heterogeneous mixed with other liquid/solid substances such as bioactive molecules or ceramic powders (Collins et al., 2008; Dash and Konkimalla, 2012; Fanovich and Jaeger, 2012; Fleming and Kazarian, 2005; Jenkins et al., 2006; Kiran, 2009; Léonard et al., 2008; Shieh and Yang, 2005; Shieh et al., 2009; Tai et al., 2007a, 2007b; Xu et al., 2004). Upon depressurization, the supersaturation of the polymer phase by CO_2 leads to the formation of porous polymeric foams as the initially trapped gas leaves the polymeric phase. The nucleation stage mostly involves the assembly of CO_2 molecules, with concurrent homogeneous and heterogeneous nucleation mechanisms occurring upon the phase separation of the polymer-CO_2 solution (Jenkins et al., 2006; Léonard et al., 2008; Tsivintzelis et al., 2007). These processes can be controlled by varying the depressurization rate and the amount of absorbed CO_2 by changing the operational temperature and pressure conditions (Collins et al., 2008). The presence of dispersed inorganic particles may affect the polymer–$scCO_2$ interactions and favor heterogeneous nucleation (thus acting as nucleation sites). This usually leads to the formation of smaller pores and to narrow pore size distribution (Collins et al., 2008, 2010; Jenkins et al., 2006; Léonard et al., 2008; Shieh et al., 2009; Tsimpliaraki et al., 2011). $scCO_2$-assisted impregnation/deposition method (SSID) is another advantageous method for precise incorporation of bioactive substances into polymeric, inorganic and composite materials in a short time and without the presence of harmful solvent residues (Ahern et al., 2012; Braga et al., 2011; Belhadj-Ahmed et al., 2009; Kazarian, 2000; Kikic and Vecchione, 2003; López-Periago et al., 2009; Natu et al, 2008). SSID permits to load previously prepared biomaterials (or even biomedical articles/devices) with the desired bioactive substances without interfering with any of the required synthesis/processing methods (Braga et al., 2008; Costa et al., 2010a, 2010b; Masmoudi et al., 2011; Yañez et al., 2011).

Poly(α-esters) (or poly(α-hydroxy acids)), such as poly(glycolic acid) (PGA), poly(lactic acid) (PLA), poly(lactic-co-glycolic acid) (PLGA) and poly(ε-caprolactone) (PCL), have attracted great attention for long-term hard tissue engineering applications due to their chemical, physical and biological properties as well as to their processability features and slow degradation rates (Burg et al., 2000; Dash and Konkimalla, 2012; Liu et al., 2008; Salgado et al., 2004). These biomaterials can be also processed by SFM, alone or in combination with bioactive substances and/or inorganic materials (Collins et al., 2008; Georgiou et al., 2007; Salerno et al., 2011; Shieh et al., 2009; Tai et al., 2007b; Teng et al., 2007; Tsimpliaraki et al., 2011; Xu et al., 2004; Zhai et al., 2006). On the other hand, inorganic silica-based materials such as mesoporous silicas, bioglasses, and silica-based composite/hybrid materials, are known to be applicable in numerous biomedical and pharmaceutical applications (Bose and Taradfer, 2012; Rahman et al., 2011; Sanchez et al., 2011; Vallet-Regí et al., 2007, 2011a, 2011b; Vivero-Escoto et al., 2010). For example, pure and functionalized mesoporous silica nanoparticles (SNPs) (such as MCM-41 and SBA-15 SNPs) have been pointed out as efficient carriers for various therapeutic and diagnostic agents (Ambrogi et al., 2012; Fuller et al., 2008; Rosenholm et al., 2010; Vallet-Regí et al., 2007; Vivero-Escoto et al., 2010). The combination of biodegradable polymeric PCL foams with biocompatible mesoporous SNPs and with bioactive substances may embody the desirable main features of hard (inorganic) and soft (organic) matter, as well as of bioactive/signaling substances, thus mimicking the original chemical, physical and biological properties of bone and dental hard tissues (Arcos and Vallet-Regí, 2010; Ogoshi and Chujo, 2005).

The aim of this work was the development of PCL/SNPs composite biomaterials that may present adequate chemical, mechanical, morphological and biological properties for hard tissue engineering applications, and which may be used alone, incorporated into other biopolymers or, alternatively, into commercially available injectable hydrogels or fast-setting bone/dental cements. PCL and mesoporous SNPs (MCM-41 and SBA-15) were processed by SFM at various proportions, $scCO_2$ density, processing time and depressurization conditions. The composites were loaded with dexamethasone (DXMT), a bioactive substance widely used as an anti-inflammatory and as an immuno-suppressant drug, as well as to enhance stem cell differentiation toward the osteogenic lineage (Kaji et al., 1997; Kim et al., 1999), by impregnation of the SNPs (using the SSID method) and later incorporation into PCL using the SFM method.

2. Materials and methods

2.1. Chemicals

Poly(ε-caprolactone) (pellets, $40\,000 \leq M_n \leq 50\,000\ g\ mol^{-1}$, $48\,000 \leq M_w \leq 90\,000\ g\ mol^{-1}$), dexamethasone (DXMT, purity ≥ 98%), methanol (purity ≥ 99%), acetone (purity ≥ 99%) and MCM-41 mesoporous silica nanoparticles (SNPs) (hexagonal; pore volume: $0.98\ cm^3\ g^{-1}$; pore sizes: 2.3–2.7 nm; surface area: $1000\ m^2\ g^{-1}$; bulk density: $0.34\ g\ cm^{-3}$) were supplied by Sigma–Aldrich. SBA-15 SNPs were provided by ClaytecInc (average pore size: 8.5 nm; pore volume: $0.93\ cm^3\ g^{-1}$; surface area: $718\ m^2\ g^{-1}$). CO_2 was obtained from Praxair (purity ≥ 99.998%). Purified water (MilliQ, Millipore, resistivity >18 MΩ cm) was obtained by reverse osmosis. Dialysis membranes ($8000\ g\ mol^{-1}$ cut-off) were supplied by Spectrum Laboratories.

2.2. Preparation of PCL powders

In order to facilitate the physical mixture of PCL with SNPs, PCL pellets were firstly dissolved in acetone ($0.0625\ g\ ml^{-1}$) and later precipitated with methanol (10 ml) and water (10 ml). PCL precipitates were filtered and dried at room temperature until constant weight. Dried PCL powders were mechanically sieved (US Mesh No. 35, sieve size 0.5 mm) down to particle diameters smaller than 500 μm.

2.3. Dexamethasone loading into SNPs

DXMT was loaded into MCM-41 and SBA-15 SNPs applying a $scCO_2$ impregnation/deposition method (SSID), using a discontinuous apparatus previously reported (Braga et al., 2011; Costa et al., 2010a, 2010b; Dias et al., 2011; Natu et al, 2008). SNPs (16 mg) were placed inside four sealed dialysis membranes which

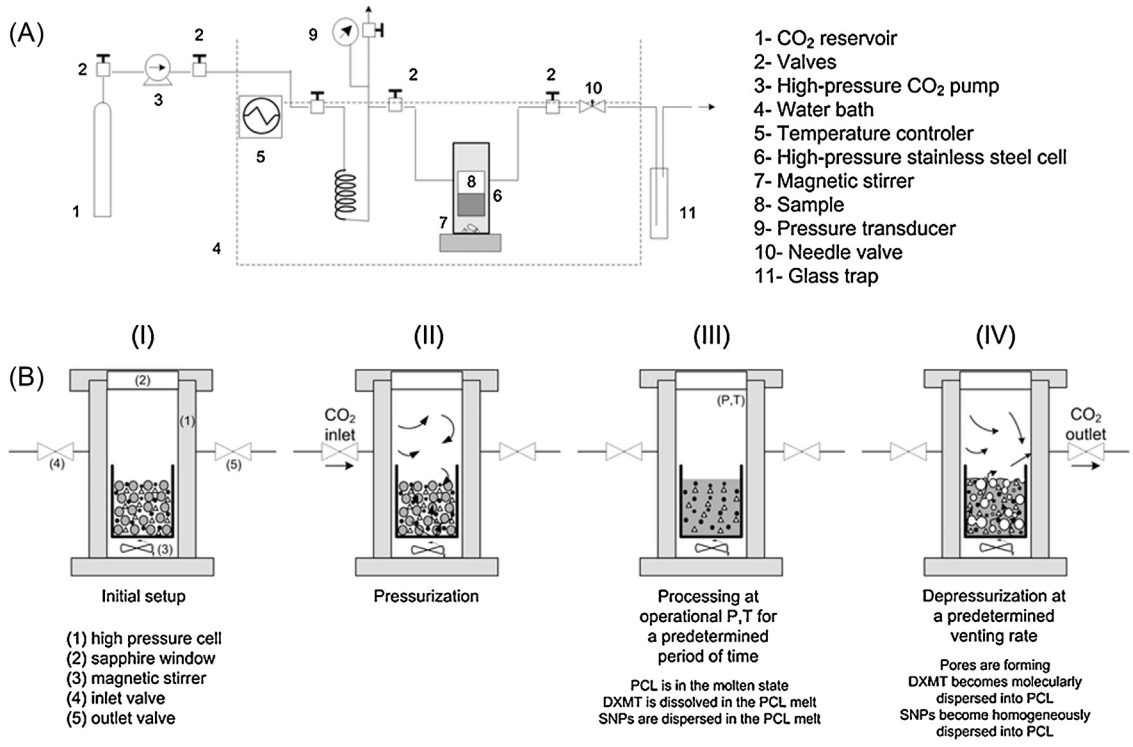

Fig. 1. The SFM process. Schematic diagram of the experimental set-up (A); Schematic representation of the occurring phases during the SFM process (B).

were introduced in a high pressure cell placed in a temperature-controlled water bath. The cell was loaded with 9 mg of DXMT (i.e., an amount 8–9 times greater than that needed to saturate $scCO_2$ under the operational conditions (Chim et al., 2012)) and CO_2 was then introduced. Experiments were performed under magnetic stirring (700 rpm) at 35 °C and at 14.0 MPa or 25.0 MPa (which corresponds to $scCO_2$ densities of 0.801 g cm^{-3} and 0.901 g cm^{-3}, respectively) (NIST, 2013). After processing periods of 2 and 14 h, the compressed fluid was removed at 0.2 dm^3 min^{-1}. Drug-loaded samples were taken out the dialysis membranes and stored in a desiccator (away from light) until further processing or analysis. All assays were performed in triplicate.

Conventional drug loading was performed, in triplicate, by immersion of MCM-41 and SBA-15 SNPs (100 mg) in 10 ml of a DXMT aqueous solution (26 μg ml^{-1}) and kept under stirring (at 100 rpm and 37 °C) for 8 h. Drug loading was followed by monitoring the decrease in the DXMT concentration in the solution (UV–vis spectrophotometry, Jasco, Model V650, Japan) for 8 h.

2.4. $scCO_2$-assisted foaming/mixing (SFM) experiments

SFM experiments were performed, in duplicate, in the same apparatus as for the SSID experiments at pressure and temperature chosen based on previous results (Léonard et al., 2008; Shieh et al., 2009; Xu et al., 2004) and taking in consideration the $scCO_2$ densities at those conditions (NIST, 2013). A schematic diagram of the experimental set-up is presented in Fig. 1(A). Prior to experiments, pre-determined amounts of PCL and MCM-41 SNPs were physically mixed in 10 ml glass vials at 70:30 and 90:10 wt%. Inner diameter of glass vials was 1.7 cm). Total sample weight was ~1.5 g. Each vial containing a solid mixture was introduced into the high pressure cell which was subsequently sealed, heated up to 35 °C and filled with CO_2 up to 14.0 MPa or 25.0 MPa (0.801 g cm^{-3} and 0.901 g cm^{-3}, respectively). Magnetic stirring (700 rpm) was used to help the homogenization of the $scCO_2$ phase. After a pre-determined processing time (2 and 14 h), the high pressure cell was depressurized down to atmospheric pressure at a fixed flow rate of 0.2 dm^3 min^{-1} or 3.0 dm^3 min^{-1}. Control samples (pure PCL, 100:0 wt%) were also processed at the above referred conditions. After processing, all samples were removed from glass vials, transferred to falcon tubes and stored in a desiccator away from light.

In other experiments, previously DXMT-loaded MCM-41and SBA-15 SNPs (by SSID) were mixed with pure PCL (70:30 and 90:10 wt%, PCL:SNPs). Total sample weight was ~300 mg. In addition, ~6 mg of DXMT (2 wt%) were added to the mixture. Samples were then processed by the SFM method at 35 °C and 14.0 MPa or 25.0 MPa for 14 h, and employing a depressurization rate of 0.2 dm^3 min^{-1}. PCL:DXMT 98:2 wt% physical mixtures (without adding SNPs) were also processed. A schematic representation of the different phases of the SFM process is presented in Fig. 1(B). All SFM-processed samples presented a cylindrical geometry, with a diameter of 1.7 cm. Before processing, solid mixtures heights were approximately 1.5 cm. However after the SFM-processing, their heights varied between 1.2 and 2.1 cm (depending on the specific employed operational conditions and initial powder mixture compositions).

2.5. Drug release experiments and kinetic analysis

DXMT release assays from samples prepared using $scCO_2$-based methods (by SSID and SFM) were performed in duplicate in water, by placing 15 mg of sample (particles or disks 2.0 mm thickness × 5.5 mm diameter) inside dialysis membranes. At pre-determined time intervals, an aliquot (3 ml) of the release media was analyzed by UV–vis spectrophotometry at 242 nm (Jasco, model V650, Japan). For DXMT-loaded SNPs, the release media was replaced every 24 h. After 72 h of release, samples were leached out in water (until no drug could be detected) and analyzed for the DXMT quantification. In the case of DXMT-loaded PCL and DXMT-loaded PCL/SNPs composites, drug release was followed for one week.

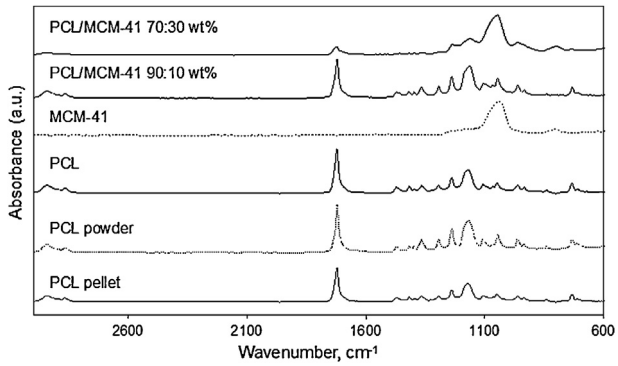

Fig. 2. FTIR-ATR spectra of PCL (pellets and powders), of processed PCL and of processed PCL/MCM-41 composites (70:30 wt% and 90:10 wt%). $scCO_2$-assisted foaming/mixing (SFM) conditions were: 25 MPa, 2 h, 3.0 $dm^3\ min^{-1}$.

The release profiles were analyzed, as for related systems (Braga et al., 2008; Dias et al., 2011; Natu et al, 2008; Yañez et al., 2011) using the Korsmeyer–Peppas model (Siepmann and Peppas, 2001; Siepmann and Siepmann, 2011):

$$\frac{M_t}{M_\infty} = kt^n \quad (1)$$

where M_t and M_∞ represent the cumulative amount of drug released at time t and at infinite time, respectively; k is a pseudo kinetic constant that incorporates the structural and geometric characteristics of the system; and n is the release exponent, which can provide some information about the involved release mechanisms.

2.6. Chemical and physical characterization

Non-processed and processed samples were characterized by means of Fourier-transform infra-red spectroscopy (FTIR-ATR), light scattering, X-ray diffraction (XRD), simultaneous differential thermal analysis (SDT), nitrogen adsorption, mercury intrusion porosimetry, helium pycnometry, mechanical compression tests and scanning electron microscopy (using image analysis of backscattered electrons (SEM-BSE)). Detailed descriptions on these assays and procedures are presented in Supplementary data, Appendix A.

3. Results and discussion

3.1. Composite characterization

3.1.1. SNPs particle sizes and particle size distributions

Two commercial mesoporous SNPs were used to prepare sponge-like composites with PCL; namely MCM-41 SNPs with diameters in the 3–2000 μm range (bimodal distribution; $d_{50} = 84.5 \pm 5.6$ μm; $d_{90} = 1167.0 \pm 58.4$ μm), and SBA-15 SNPs with sizes in the 3–200 μm range (unimodal distribution; $d_{50} = 34.9 \pm 0.4$ μm; $d_{90} = 83.4 \pm 0.9$ μm).

3.1.2. Fourier-transform infra-red spectroscopy (FTIR-ATR)

The presence of both components was confirmed by FTIR-ATR (Fig. 2). The characteristic PCL crystalline phase peaks appeared at 1727 cm^{-1} (carbonyl group stretching) and 1293 cm^{-1} (C—O and C—C stretching) (Elzubair et al., 2006; Elzein et al., 2004; Kweon et al., 2003), and those of the mesoporous/amorphous silica (MCM-41) at 1090 and 1223 cm^{-1} due to the Si—O asymmetric stretching and at 800 cm^{-1} because of Si—O symmetric stretching (Fidalgo and Ilharco, 2001; Prakash et al., 1995). In the 70:30 wt% PCL/MCM-41 composites, the peaks of both components were seen. In the case of 90:10 wt% PCL/MCM-41 composites, the peaks of mesoporous/amorphous silica could not be distinguished, because of the low proportion of MCM-41 SNPs and their dispersion into the PCL matrix. Nevertheless, the presence of MCM-41 SNPs was confirmed by SEM-EDX for all prepared PCL/MCM-41 composites (Supplementary data, Appendix B, Fig. S.I. 1). As expected, no apparent chemical modifications were observed in PCL after SFM.

3.1.3. Thermal analyses (SDT)

Thermogravimetric analysis (SDT) of 70:30 wt% PCL/MCM-41 samples (processed at all experimental conditions) showed a total weight loss of 68–74% at 700 °C (Supplementary data, Appendix C, Table S.I. 1). For 90:10 wt% PCL/MCM-41 samples and processed pure PCL, the weight losses were 87–95% and 99.0–99.8%, respectively. Therefore, the SFM method led to PCL/MCM-41 composites that matched the feed compositions. SDT runs (Fig. 3 and Supplementary data, Appendix C, Table S.I. 1) also showed double melting peaks (or one main melting peak with a shoulder) for all analyzed samples containing PCL (before and after SFM processing), which means that they underwent a crystallization process (during pellet production by manufacturer, during the initial PCL powder preparation, and during the SFM process – at all conditions) (Kiran et al., 2008). While the supplier reports PCL melting temperature value in the 56–64 °C range, the obtained SDT results indicated slightly higher values (~67–68 °C). By contrast, the SFM processing seems to lower the PCL melting temperature (~65 °C), particularly for the higher processing pressure (25 MPa), which suggests that the employed process decreased PCL crystallinity. Similar and opposite effects were previously reported in the literature (Kiran et al., 2008; Shieh and Yang, 2005; Salerno et al., 2011). These discrepancies can be explained by the use of PCLs with different properties (such as polymer average molecular weight, molecular weight distribution and original polymer crystallinity), and by the formation of different lamellar thicknesses and crystal heterogeneity (during the crystallization process and as the result of the processing temperatures and pressures). The incorporation of MCM-41 SNPs during $scCO_2$ processing also seems to induce a further decrease in the PCL melting temperature, as previously reported for calcium hydroxyapatite nanoparticles (Salerno et al., 2011) and for natural extracts (Fanovich et al., 2013). PCL degradation temperature remained almost constant for all processed samples, except for those containing the highest MCM-41 proportion (70:30 wt%) for which a decrease was observed. Therefore, PCL thermally induced degradation seems to be favored by the presence of MCM-41 SNPs (Chrissafis et al., 2007; Fukushima et al., 2009; Molinaro et al., 2013). In sum, the melting temperatures are above the physiological temperature, while the degradation temperatures are greatly above the typical polymeric processing temperatures, which makes these materials suitable for biomedical applications and easily processable at temperatures below 100–150 °C (without degradation).

3.1.4. X-ray diffraction (XRD)

XRD patterns obtained for PCL pellets/powders and for a few selected $scCO_2$-processed samples (14 and 25 MPa, for 14 h, and depressurized at 3.0 $dm^3\ min^{-1}$) PCL and PCL/MCM-41 composites (70:30 wt%) are shown in Supplementary data (Appendix D, Figure S.I. 2). PCL diffractograms usually present a broad peak at approximately 18° (amorphous regions) and other peaks at 25° and at 27.7° (crystalline regions): diffraction planes (1 1 0) and (2 0 0), respectively [72–74]. Similar diffraction patterns were obtained for the non-processed PCL pellets/powders. However, peaks deconvolution and analysis showed a significant difference in crystallinity: 52.0% (for pellets) and 68.7% (for powder). This difference can be due to the different diffraction planes orientations of powders and pellets (they are the same material but they were processed by different methods). For the $scCO_2$-processed PCL samples, it was

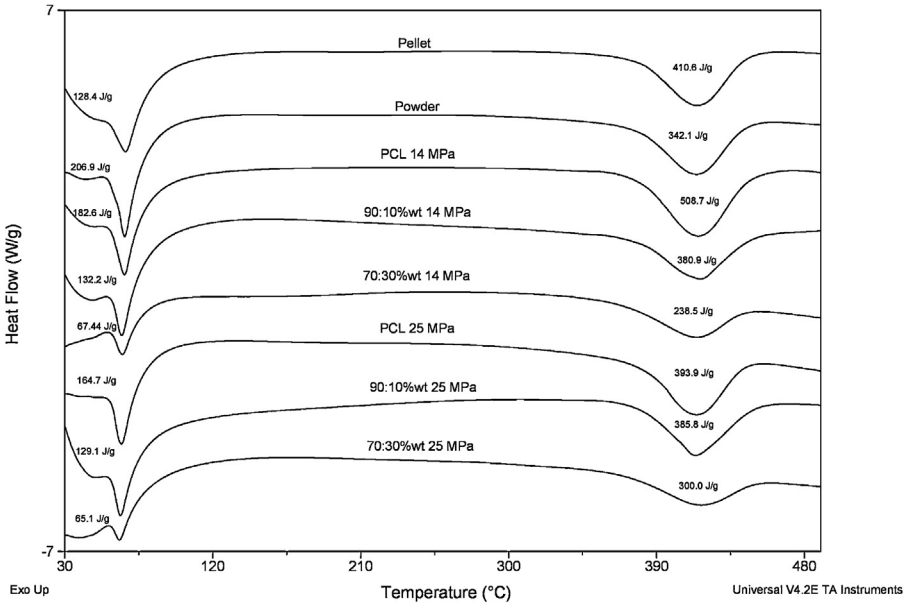

Fig. 3. Calorimetric profiles of PCL (pellets and powders), of processed PCL and of processed PCL/MCM-41 composites (70:30 wt% and 90:10 wt%). $scCO_2$-assisted foaming/mixing conditions (SFM) were: 2 h and 3.0 dm h and 3.0 $dm^3\ min^{-1}$. Melting and degradation enthalpies are indicated.

observed a decrease in peak intensities and a broadening of the "crystalline" peaks (at 25° and 27.7°). Deconvolution analysis indicated that the crystallinity degree decreased when samples were processed at 14 MPa (56.7%), and remained nearly constant when samples were processed at 25 MPa (69.4%). The addition of inorganic particles into PCL (70:30 wt% PCL/MCM-41 samples) and its further $scCO_2$-processing led to a clear PCL crystallinity degree (around 40%, for both processing pressures). This occurs because the inorganic particles will hamper the formation of large PCL crystallites (as it would happen in the absence of the inorganic filler) (Jiang et al., 2001; Messersmith and Giannelis, 1995).

3.1.5. Scanning electron microscopy (SEM)

The different MCM-41 compositions and operational conditions led to samples presenting quite distinct microscopic morphologies (Figs. 4 and 5). Pure PCL samples processed at 14 MPa for 14 h (Fig. 4) showed smaller pores and "denser" structures. Samples processed for 2 h exhibited different types of pores: from small up to much larger pores (that seem to be interconnected). It is known that hard-tissue engineering applications require large and interconnected macropores (between 200 and 900 μm and between 1.2 and 2.0 mm) for cell/nutrient diffusion and vascularization, as well as micropores and mesopores (smaller than 2 nm and between 2 nm and 50 nm, respectively) for fast degradability and efficient loading, transport and release of bioactive substances (Burg et al., 2000; Holly et al., 2000; Salgado et al., 2004). For the same processing periods (2 h or 14 h), faster depressurization rates (3 $dm^3\ min^{-1}$) promoted the formation of more and smaller pores. On the other hand, the addition of MCM-41 SNPs (90:10 wt%) led to the formation of more pores particularly bigger for samples processed for 14 h. For higher MCM-41 contents (70:30 wt%), "dense" and "agglomerated" macrostructures were obtained for all the operational conditions. Comparable macroscopic morphologies were obtained for the samples processed at 25 MPa (Fig. 5), at the same processing time, depressurization rate and MCM-41 proportion. Only for impure PCL samples, a decrease in pore sizes was macroscopically observed after processing at 25 MPa, as previously found in similar systems (Collins et al., 2008; Fanovich and Jaeger, 2012; Jenkins et al., 2006; Léonard et al., 2008; Salerno et al., 2011; Tai et al., 2007b). In the absence of inorganic particles, higher pressure allows more gas molecules to be absorbed by the polymer, which consequently leads to the formation of more nucleation sites (higher nucleation density) and smaller pores.

3.1.6. Nitrogen adsorption, mercury intrusion porosimetry and helium pycnometry

Helium pycnometry, mercury intrusion and nitrogen adsorption, were applied for accurate characterization of the porosity (Table 1). For both pressures (14 and 25 MPa), real density of composites increased with the proportion of MCM-41 SNPs from 1.13 up to 1.31 g cm^{-3}, because MCM-41 real density is greater (2.0–2.6 g cm^{-3}, Collins et al., 2008) than that of pure PCL (1.1–1.2 g cm^{-3}, Collins et al., 2008; Fanovich and Jaeger, 2012). Operational conditions (pressure, processing time and depressurization rate) had a small or no evident effect on the real density values (for PCL and PCL/MCM-41 composites), despite slightly lower values were obtained after processing at 14 MPa. Apparent density determined by mercury intrusion porosimetry was between 1.11 and 1.18 g cm^{-3} for pure PCL, and between 0.90 and 1.24 g cm^{-3} for PCL/MCM-41 composites. These values are similar to those obtained using helium pycnometry and follow the same trends with the increasing MCM-41 composition and with the employed operational conditions.

Bulk density varied between 0.60 and 1.01 g cm^{-3} for pure PCL, and between 0.49 and 0.97 g cm^{-3} for PCL/MCM-41 composites and, in general, decreased as the MCM-41 proportion increased (for all the tested operational conditions). This happens because of the quite low bulk density of MCM-41 (0.34 g cm^{-3}). Processing times and depressurization rates did not exert evident effect on bulk density, but high pressure processing (25 MPa) led to slightly lower bulk density values.

The porosity became higher with the increase of the MCM-41 proportion (for 14 and 25 MPa), which confirms the above explained bulk density trends. In addition, MCM-41 SNPs provided more nucleation points during the system depressurization that resulted in final higher porosities. Fast depressurization rates rendered less porous PCL and 90:10 wt% PCL/MCM-41 composites, as previously reported for PLA scaffolds (Collins et al., 2008). This variable did not affect the porosity of composites with higher MCM-41 content (70:30 wt%). Operational pressures and processing times

Table 1
Morphology results obtained for $scCO_2$-processed PCL and PCL/MCM-41 composites.

PCL/MCM-41			Nitrogen adsorption			Mercury intrusion				Helium pycnometry
Processing conditions			Surface area ($m^2\,g^{-1}$)	Pore volume ($cm^3\,g^{-1}$) ($\times 10^3$)	Average pore diameter (Å)	Average pore diameter (μm)	Porosity (%)	Apparent density ($g\,cm^{-3}$)	Bulk density ($g\,cm^{-3}$)	Real density ($g\,cm^{-3}$)
Pure PCL 14 MPa	2 h	0.2 $dm^3\,min^{-1}$	0.91 ± 0.23	1.56 ± 0.28	68.60 ± 5.07	0.11 ± 0.02	51.90 ± 2.93	1.18 ± 0.02	0.99 ± 0.01	1.26 ± 0.01
		3.0 $dm^3\,min^{-1}$	0.62 ± 0.03	1.44 ± 0.48	72.96 ± 12.35	0.07 ± 0.01	11.88 ± 0.85	1.13 ± 0.01	0.76 ± 0.28	1.24 ± 0.01
	14 h	0.2 $dm^3\,min^{-1}$	0.83 ± 0.04	1.75 ± 0.18	85.97 ± 13.91	0.40 ± 0.08	17.26 ± 2.19	1.14 ± 0.01	1.00 ± 0.01	1.25 ± 0.01
		3.0 $dm^3\,min^{-1}$	0.65 ± 0.05	1.58 ± 0.02	96.58 ± 6.07	0.09 ± 0.01	16.12 ± 0.36	1.13 ± 0.02	0.71 ± 0.27	1.27 ± 0.02
90:10 wt% 14 MPa	2 h	0.2 $dm^3\,min^{-1}$	1.95 ± 0.06	4.60 ± 1.78	130.13 ± 16.56	0.25 ± 0.05	43.66 ± 1.90	1.23 ± 0.01	0.63 ± 0.05	1.15 ± 0.01
		3.0 $dm^3\,min^{-1}$	1.74 ± 0.44	5.49 ± 2.43	76.23 ± 10.04	0.14 ± 0.04	26.40 ± 0.64	1.13 ± 0.01	0.64 ± 0.03	1.15 ± 0.01
	14 h	0.2 $dm^3\,min^{-1}$	1.91 ± 0.28	5.20 ± 2.28	140.74 ± 0.67	0.22 ± 0.02	40.20 ± 0.20	1.16 ± 0.02	0.90 ± 0.09	1.13 ± 0.02
		3.0 $dm^3\,min^{-1}$	1.27 ± 0.11	2.43 ± 0.59	79.26 ± 28.39	0.11 ± 0.02	16.35 ± 0.96	1.13 ± 0.01	0.68 ± 0.01	1.15 ± 0.01
70:30 wt% 14 MPa	2 h	0.2 $dm^3\,min^{-1}$	20.54 ± 0.67	39.87 ± 2.14	77.63 ± 1.64	0.73 ± 0.28	50.53 ± 3.47	1.05 ± 0.10	0.52 ± 0.02	1.26 ± 0.01
		3.0 $dm^3\,min^{-1}$	16.56 ± 2.96	28.63 ± 10.16	53.59 ± 0.37	0.21 ± 0.03	48.57 ± 3.68	1.20 ± 0.03	0.62 ± 0.06	1.24 ± 0.01
	14 h	0.2 $dm^3\,min^{-1}$	13.36 ± 1.82	27.21 ± 12.16	111.76 ± 22.18	6.80 ± 1.24	49.49 ± 2.79	1.20 ± 0.03	0.62 ± 0.06	1.25 ± 0.01
		3.0 $dm^3\,min^{-1}$	11.18 ± 1.56	14.64 ± 0.38	52.80 ± 6.01	0.32 ± 0.01	48.70 ± 3.79	1.13 ± 0.15	0.57 ± 0.05	1.27 ± 0.02
Pure PCL 25 MPa	2 h	0.2 $dm^3\,min^{-1}$	0.78 ± 0.08	1.56 ± 0.01	80.32 ± 5.69	0.24 ± 0.02	45.42 ± 1.37	1.15 ± 0.02	0.83 ± 0.03	1.10 ± 0.01
		3.0 $dm^3\,min^{-1}$	0.52 ± 0.04	0.89 ± 0.23	68.34 ± 11.74	0.09 ± 0.01	11.92 ± 1.65	1.11 ± 0.02	0.60 ± 0.03	1.13 ± 0.02
	14 h	0.2 $dm^3\,min^{-1}$	0.65 ± 0.06	1.42 ± 0.01	87.64 ± 3.54	0.09 ± 0.01	22.09 ± 1.00	1.14 ± 0.01	1.01 ± 0.03	1.10 ± 0.02
		3.0 $dm^3\,min^{-1}$	0.65 ± 0.08	0.89 ± 0.42	59.04 ± 9.93	0.08 ± 0.01	16.36 ± 0.90	1.14 ± 0.01	0.89 ± 0.01	1.12 ± 0.01
90:10 wt% 25 MPa	2 h	0.2 $dm^3\,min^{-1}$	2.21 ± 0.39	7.03 ± 0.78	130.54 ± 37.28	0.26 ± 0.04	43.62 ± 1.59	1.22 ± 0.01	0.55 ± 0.01	1.14 ± 0.01
		3.0 $dm^3\,min^{-1}$	1.33 ± 0.60	2.27 ± 0.66	70.98 ± 12.13	0.15 ± 0.02	21.99 ± 0.62	1.16 ± 0.01	0.65 ± 0.02	1.16 ± 0.01
	14 h	0.2 $dm^3\,min^{-1}$	15.19 ± 0.57	29.69 ± 7.93	60.50 ± 1.83	0.26 ± 0.03	50.37 ± 5.90	1.16 ± 0.01	0.90 ± 0.01	1.17 ± 0.02
		3.0 $dm^3\,min^{-1}$	39.59 ± 16.23	44.41 ± 14.60	45.68 ± 3.98	0.12 ± 0.01	27.54 ± 1.55	1.13 ± 0.04	0.56 ± 0.09	1.17 ± 0.01
70:30 wt% 25 MPa	2 h	0.2 $dm^3\,min^{-1}$	17.50 ± 5.99	29.56 ± 4.10	65.07 ± 26.44	0.32 ± 0.04	55.37 ± 0.33	1.15 ± 0.01	0.97 ± 0.01	1.27 ± 0.01
		3.0 $dm^3\,min^{-1}$	68.84 ± 27.78	85.57 ± 32.22	50.01 ± 1.45	39.45 ± 8.32	46.17 ± 1.59	1.24 ± 0.01	0.55 ± 0.01	1.31 ± 0.02
	14 h	0.2 $dm^3\,min^{-1}$	75.24 ± 9.31	92.17 ± 20.81	42.76 ± 0.68	1.50 ± 0.25	47.58 ± 2.32	0.90 ± 0.06	0.49 ± 0.02	1.31 ± 0.01
		3.0 $dm^3\,min^{-1}$	134.70 ± 5.58	151.13 ± 51.49	41.33 ± 3.89	0.22 ± 0.08	55.23 ± 0.05	0.98 ± 0.10	0.51 ± 0.03	1.29 ± 0.01

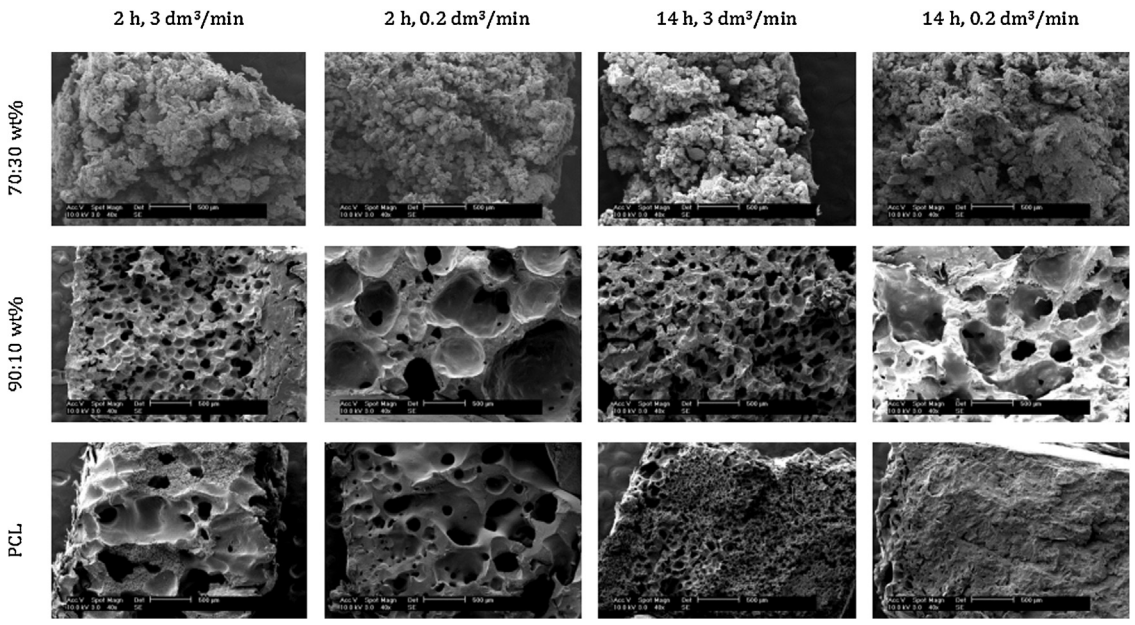

Fig. 4. SEM analysis for PCL and $scCO_2$-assisted PCL-MCM-41 composites processed at 14 MPa. Magnification 40×. Scale bar 500 μm.

did not have a comprehensible effect on the obtained porosity results, despite other authors reported that porosity can be favored by longer processing times (Tai et al., 2007b). As expected, surface areas and pore volumes (determined by nitrogen adsorption) increase with the increasing MCM-41 proportion (for all tested pressure, processing time and depressurization conditions). This is due to the high surface areas and pore volumes of MCM-41 SNPs (1000 $m^2\ g^{-1}$ and 0.98 $cm^3\ g^{-1}$, respectively – data provided by supplier) and is in agreement with the above presented bulk density and porosity results. Average pore diameters were measured by nitrogen adsorption (0.5–100 nm; micro and mesopores) and mercury intrusion porosimetry (4 nm–850 μm; meso and macropores). Nitrogen adsorption led to average pore diameters of 5.9–9.7 nm for pure PCL and of 4.1–14 nm for PCL/MCM-41 composites. In general, the average pore diameters decreased as the MCM-41 proportion increased, due to the introduction into the composites of the SNPs that possess average pore diameters between 2.3 and 2.7 nm, in agreement with previous results (Collins et al., 2008; Holly et al., 2000; Tsimpliaraki et al., 2011). Average pore diameters were also smaller for composites processed at 25 MPa. Pressure effect was not observed for pure PCL samples, despite the fact that other authors found that larger pores are formed with higher processing pressures (Xu et al., 2004). On the other hand, the average pore diameters obtained by mercury intrusion were found to be in the 80–400 nm range for pure PCL and in the 110 nm–39.5 μm for PCL/MCM-41 composites. The size of the macropores increased with the MCM-41 proportion (for all tested operational conditions), which can be explained by the fact that the introduction of MCM-41 SNPs affects the nucleation of CO_2 inside the PCL matrices and thus leads to larger pore diameters than those obtained for pure PCL. In general, pressure and processing time did not present comprehensible effects and tendencies, contrarily to faster depressurization

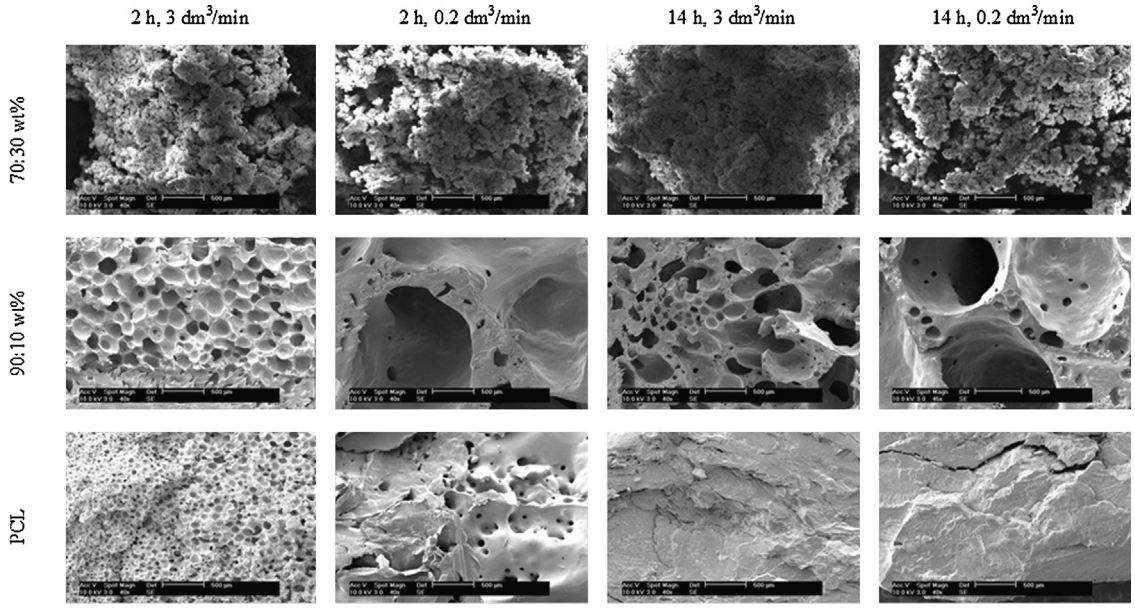

Fig. 5. SEM analysis for PCL and $scCO_2$-assisted PCL-MCM-41 composites processed at 25 MPa. Magnification 40×. Scale bar 500 μm.

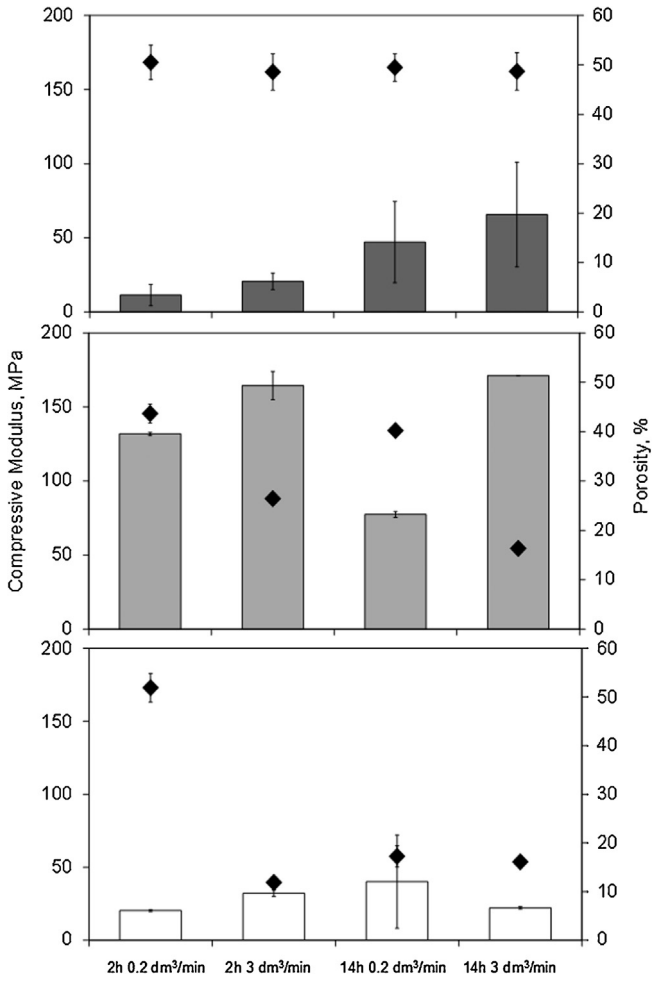

Fig. 6. Compressive modulus (at a 10% strain) (bars) and porosities (♦) of PCL and PCL/MCM-41 samples processed at 14 MPa: 70:30 wt%, top (■); 90:10 wt%, middle (▩); and pure PCL, bottom (□).

rates that led to smaller average pore diameters (at all operational conditions and for all tested PCL and PCL/MCM-41 samples – as previously observed by SEM). This is mostly due to the CO_2 diffusion rate in the molten polymer and similar results were already reported in the literature (Collins et al., 2010; Fanovich and Jaeger, 2012; Jenkins et al., 2006; Kiran, 2010; Tai et al., 2007b; Xu et al., 2004; Zhai et al., 2006).

In sum, the implemented SFM method enables the preparation of PCL and PCL/MCM-41 composite biomaterials with different morphological properties (density, porosity, surface area, pore volume, average pore diameter and pore diameter range) simply by changing some of the processing conditions (pressure, processing time and depressurization rate, Chen et al., 2002; Tai et al., 2007b; Teng et al., 2007; Rouholamin et al., 2013) and the MCM-41 relative composition.

3.1.7. Mechanical compression tests

Other properties, such as mechanical properties (Fig. 6 and Supplementary data, Appendix E, Table S.I. 2) may also be affected by these processing strategies. Compressive moduli and compressive stresses increased ~30% and ~15%, respectively, when 10 wt% of MCM-41 SNPs were added to PCL. However, further increase in SNPs proportion up to 30 wt% caused the compressive moduli (and stresses) to decrease to values similar to those of PCL samples. Therefore, the addition of 10 wt% of this inorganic filler reinforced PCL structure, but a further increase in its proportion led to the opposite effect. Similar results were described for other composite materials (Georgiou et al., 2007; Lee et al., 2005; Mathieu et al., 2005) and attributed to the higher heterogeneity and increased porosity of composites having high contents of porous inorganic materials, which increases the phase separation and impairs the interaction/compatibility between composite inorganic/organic counterparts, thus leading to lower compressive moduli (Mathieu et al., 2005). Effects of pressure, processing time and depressurization rate were not evident, although lower compressive moduli and compressive stresses were obtained for pure PCL samples processed at the highest pressure condition (25 MPa). In sum, PCL samples and PCL/MCM-41 composites presented compressive modulus lower than those characteristic of trabecular and cortical bone (ca. 0.1–5 GPa and 10–20 GPa, respectively) (Baker et al., 2009; Fu et al., 2011; Georgiou et al., 2007). Nevertheless, mechanical properties values comparable to those of natural bones could be attained if the prepared materials are comminuted and introduced into, for example, fast-setting bone/dental cements.

3.2. Dexamethasone loading/release results

3.2.1. Dexamethasone loading

$scCO_2$-assisted loading of DXMT was carried out applying two approaches: (i) addition of known amounts of DXMT to the solid PCL/SNPs physical mixtures before SFM processing and (ii) impregnation/deposition (SSID) of DXMT into MCM-41 and SBA-15 SNPs before mixing with PCL and applying SFM processing. Additionally, soaking of the SNPs in aqueous solutions of DXMT was assayed for comparison.

In recent years our research group applied SSID to incorporate several bioactive substances into a wide range of polymers and polymer-based devices which were envisaged for distinct pharmaceutical and biomedical applications (Braga et al., 2011, 2008; Costa et al., 2010a, 2010b; Dias et al., 2011, 2013; Duarte et al., 2006, 2007; González-Chomón et al., 2012; Yañez et al., 2011). In these works, the loading yields of the SSID method were discussed in terms of the employed operational conditions (temperature, pressure, processing time, depressurization rate, and co-solvent addition) as well as of the relative and mutual physicochemical interactions that may be established between all substances involved in the process. Other authors already reported the SSID deposition of several substances into mesoporous materials and namely into mesoporous SNPs (Ahern et al., 2012; Belhadj-Ahmed et al., 2009; Kikic et al., 1996; Morère et al., 2011; Ni et al., 2012). Solid inorganic matrices cannot swell with $scCO_2$ and therefore the specific physicochemical SNPs/$scCO_2$ interactions are not relevant for the process. However, their microstructural properties (namely surface area, porosity and average pore diameter) may affect the $scCO_2$ diffusion into/out from SNPs and the corresponding deposition/adsorption yields.

The DXMT solubility in $scCO_2$ at 35 °C was found to be low and not dependent on pressure: 9.07×10^{-2} μg cm^{-3} at 15 MPa, and 10.14×10^{-2} μg cm^{-3} at 25 MPa (Chim et al., 2012). Therefore, the loading yield should be mostly controlled by the balance between the DXMT/$scCO_2$ interactions (hydrophobic methyl/CO_2 and Lewis basic-type carbonyl/CO_2) (Kazarian, 2000; Kikic, 2009; Kikic and Vecchione, 2003) and the DXMT/SNPs specific interactions (hydrogen bonds between the silanol moieties of silica and the hydroxyl groups of the DXMT molecule), which determines the final DXMT "solubility" and partitioning into SNPs. If the DXMT/$scCO_2$ interactions are not intense (like it seems to be the case), DXMT may have a high partition coefficient in SNPs and thus it could be easily deposited from the $scCO_2$ mobile phase.

Total amounts of loaded DXMT into MCM-41 and SBA-15 SNPs, estimated after complete drug leaching (for samples processed by SSID) or by monitoring aqueous DXMT concentration (soaked in aqueous solution at 37 °C) are shown in Fig. 7. DXMT loading yields

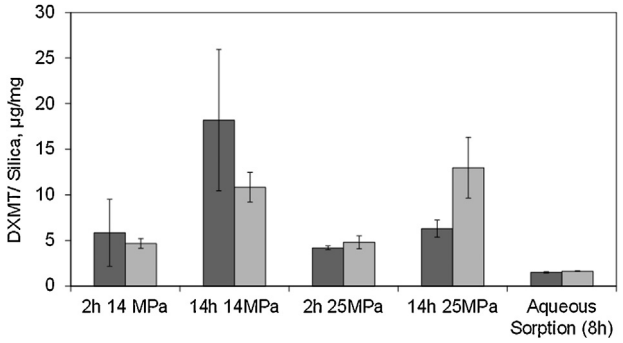

Fig. 7. Total amounts of loaded DXMT into SNPs. Loaded amounts were determined after complete drug leaching (for samples processed by SSID) and by following DXMT concentration (for samples processed by sorption from aqueous DXMT solutions). SSID experiments were carried out at different operational conditions: depressurization rate was 0.2 $dm^3\ min^{-1}$; processing times were 2 h and 14 h; and pressures were 14 MPa and 25 MPa. (■) MCM-41; (■) SBA-15.

by SSID increased with processing time (14 h vs. 2 h) for both operational pressures (14 and 25 MPa) and tested materials (MCM-41 and SBA-15). This indicates that transport properties are, in some way, affecting the DXMT loading process. For a 2-h processing period, the operational pressure does not have any clear effect on the loading yields (for both materials). However, for a 14-h processing period, the higher pressure (25 MPa) led to a lower DXMT loading yield for MCM-41, while for SBA-15 a slightly higher loading yield was observed. At 14 MPa and 35 °C, $scCO_2$ presents enhanced transport properties, i.e., a lower viscosity (~71.2 μPa s) and a higher self-diffusion coefficient ($\sim 2.1 \times 10^{-8}\ m^2\ s^{-1}$) than at 25 MPa and 35 °C (~91.7 μPa s and $\sim 1.7 \times 10^{-8}\ m^2\ s^{-1}$) (NIST, 2013; Higashi et al., 2000). Therefore, transport properties are probably not an important issue at the lower pressure condition and higher loading yields are obtained for the material having the higher surface area (MCM-41), i.e., the DXMT–silica interactions seem to be controlling the process.

However, at 25 MPa the transport properties become less favorable as $scCO_2$ viscosity increases and $scCO_2$ self-diffusion coefficient and diffusivity decreases. To the best of our knowledge, there is no literature data regarding the diffusivity of $scCO_2$ inside MCM-41 SNPs at the experimental conditions employed in this work. Diffusivity was calculated to be $\sim 1.45 \times 10^{-8}\ m^2\ s^{-1}$ (25 °C, atmospheric pressure) by molecular simulation studies (Williams et al., 2011). This CO_2 self-diffusion coefficient (inside the pores of MCM-41) is much lower than the gaseous CO_2 self-diffusion coefficient at 25 °C and atmospheric pressure ($\sim 13.8 \times 10^{-6}\ m^2\ s^{-1}$) (Massman, 1998). This fact was attributed to the interactions that may be established between CO_2 and the hydroxyl groups at the MCM-41 surface as well as to the tendency of CO_2 to become trapped in nooks in the amorphous pore walls (Williams et al., 2011). It is expected that similar phenomena may also occur at the higher pressure conditions employed in this work and for both tested SNPs (MCM-41 and SBA-15). The smaller average pore diameters of MCM-41 (if compared to those of SBA-15) may be imposing additional transport restrictions to the DXMT/$scCO_2$ mobile phase or even clogging pores apertures with deposited DXMT, thus leading to lower global DXMT loading yields into MCM-41.

DXMT loading yields by soaking of MCM-41 and SBA-15 SNPs in aqueous solutions were much lower than those attained with SSID; these differences being bigger for longer SSID processing time (14 h). The DXMT equilibrium solubility in water is 100 $\mu g\ cm^{-3}$ at 25 °C and 116 $\mu g\ cm^{-3}$ at 37 °C (Pitha et al., 1986; Yalkowsky and He, 2003). The concentration of the employed DXMT aqueous solution was 26 $\mu g\ cm^{-3}$, i.e., lower than the aqueous equilibrium solubility but much higher than the DXMT equilibrium solubility in $scCO_2$ (at the employed SSID experimental conditions). Therefore, it can be concluded that the higher loading yields obtained by the SSID method are due to the enhanced transport properties (viscosity and diffusivity) of the $scCO_2$ mobile phase (and if compared to the mobile aqueous phase). At the loading conditions by soaking in DXMT aqueous solution (37 °C and atmospheric pressure), the water viscosity (~691.5 μPa s) is much higher than the $scCO_2$ viscosity at the SSID loading conditions. Moreover, the self-diffusion coefficients of water are also lower than those of $scCO_2$. The self-diffusion coefficients of liquid water inside MCM-41 SNPs pores were found to be between $\sim 0.17 \times 10^{-10}$ and $\sim 2.3 \times 10^{-10}\ m^2\ s^{-1}$ (depending on pore diameter), which are smaller than those of bulk liquid water ($\sim 2.0 \times 10^{-9}\ m^2\ s^{-1}$) because of the strong interactions between the mobile phase molecules and the hydroxyl groups at the MCM-41 pore surfaces (as in the case of $scCO_2$) (Hansen et al., 1995). Similar results should be expected for the SBA-15 SNPs (despite their larger average pore diameters).

3.2.2. Dexamethasone release

DXMT release profiles from the MCM-41 and SBA-15 SNPs that were processed by the SSID method are shown in Fig. 8. DXMT-loaded SBA-15 SNPs released higher amounts (2.8–3.0 $\mu g\ mg^{-1}$) than MCM-41 SNPs (1.3–2.0 $\mu g\ mg^{-1}$). SBA-15 SNPs released at 8 h between 21% and 64% of the total loaded amounts, while MCM-41 SNPs only released between 10% and 44%. These results are related to the larger pore diameters of SBA-15 SNPs which help water diffusion into pores and lead to faster DXMT desorption and release. Thus, the SSID method proved to be more efficient than the aqueous sorption method to load (and release) different amounts of DXMT simply by controlling the operational conditions and/or by using different types of SNPs having distinct morphological features.

The release profiles from DXMT-loaded PCL and DXMT-loaded PCL/SNPs composites and the corresponding release kinetic parameters are shown in Fig. 9 and Table 2, respectively. In general, PCL samples released lower DXMT amounts than PCL/SNPs composites. PCL and PCL/SBA-15 samples processed at 25 MPa led to higher released amounts than those processed at 14 MPa. The processing pressure effect was not so evident in the case of PCL/MCM-41 composites. PCL/SBA-15 70:30 wt% composites released more DXMT than the 90:10 wt% composites (for both operational pressures). This compositional effect was not clear for PCL/MCM-41 samples. These findings are related to the already discussed lower bulk density and higher porosity/surface area (as well as to the different pore diameter ranges) that were obtained by increasing the operational pressure and the SNPs proportion. All these features facilitate water diffusion into samples pores which, in turn, accelerates DXMT desorption and release. PCL hydrolytic degradation should not affect DXMT release profiles due to the relatively short release period that was tested.

Regarding the release kinetics (Table 2), the higher k values were obtained for PCL/SNPs composites processed at the highest pressure condition (25 MPa). Moreover, k values for the 70:30 wt% samples were always higher than those of the 90:10 wt% samples for PCL/SBA-15 composites at both operational pressures. Once again, this compositional effect was not observed for the PCL/MCM-41 composites. Despite the lower released amounts after the 8 days, it can also be concluded that the DXMT release is faster (at initial times) for PCL samples than for PCL/SNPs. Correlated release exponents, n, which usually provide some information regarding the involved release mechanisms, were above 0.5 except for PCL and the 90:10 wt% PCL/SBA-15 composites, processed at 25 MPa, which presented slightly lower values (however, fairly close to 0.5). These results indicate that drug release was mostly controlled by an anomalous transport mechanism (i.e., a superposition of Fickian- and of Case II-type transport mechanisms) probably due to the release of the DXMT located at near-surface regions and to

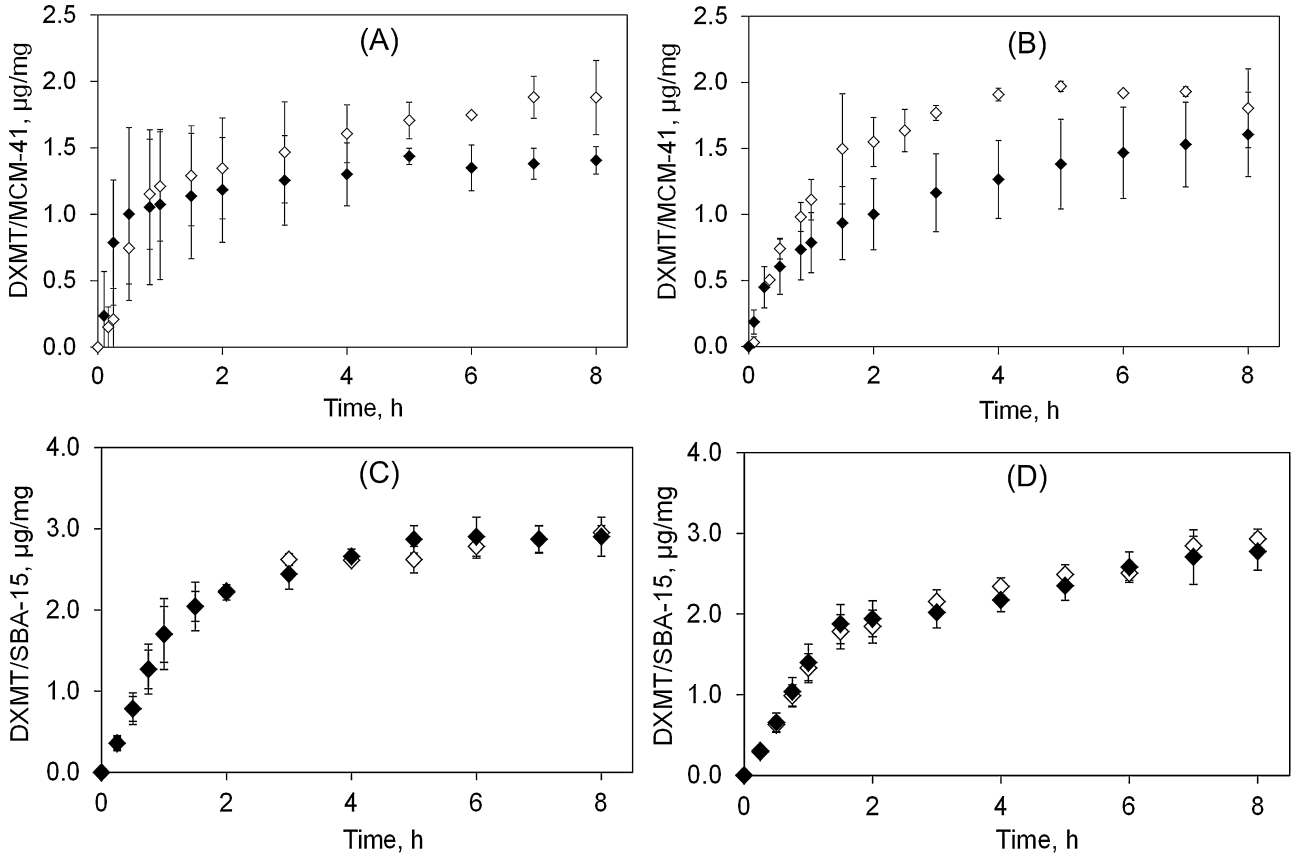

Fig. 8. DXMT release profiles from SNPs (processed by SSID). Release results are shown up to an 8 h release period for MCM-41 (top) and SBA-15 (bottom). SNPs were loaded with DXMT at different operational conditions: depressurization rate was 0.2 $dm^3\ min^{-1}$; processing times were 2 h (empty markers) and 14 h (filled markers); and pressures were 14 MPa (A and C) and 25 MPa (B and D).

the initial PCL surface skin erosion (Siepmann and Peppas, 2001; Siepmann and Siepmann, 2011).

Therefore and besides the already discussed wide range of thermomechanical and morphological properties of the processed composites, the SFM method provided a large range of distinct DXMT release profiles, which can be easily tuned by changing the process operational pressure and the type/composition of the DXMT-loaded SNPs. Although not tested in this work, it is obvious that other conditions (such as temperature, depressurization rate and processing time) may also affect the DXMT release behavior from these systems. The long-term PCL degradation should make the DXMT-loaded SNPs gradually accessible to release their cargo enabling prolonged release. It should be noticed that the prepared composite disks can be grinded down to an adequate particle size in order to be used alone or, alternatively, to be incorporated into other biopolymers, injectable hydrogels or bone/dental cements. Although biocompatibility/toxicity tests were not performed in this work, there are already evidences that all the involved chemical substances (DXMT, PCL, SNPs and CO_2) are physiologically safe, accepted and in-use for several tissue engineering and/or drug delivery applications (Fruijtier-Pölloth, 2012; Jaganathan and Godin, 2012; Schantz et al., 2004). Nevertheless, some of these tests should be performed in the near future, namely to verify the DXMT loading/release amounts that are optimal for stem cell differentiation toward the osteogenic lineage (without inducing cell toxicity).

Table 2
Correlated kinetic parameters for the DXMT release from PCL and PCL/SNPs composites, processed at 14 MPa and 25 MPa, for 14 h and depressurized at 0.2 $dm^3\ min^{-1}$. Disk/slab-shaped samples: 2.0 mm × 5.5 mm (thickness × diameter).

Samples			Kinetic parameters			Released DXMT (%)
			n	k, $days^{-n}$	R^2	
PCL		14 MPa	0.5728	0.5004	0.9504	1.9 ± 0.7
		25 MPa	0.4335	0.5053	0.9710	2.8 ± 0.1
MCM-41	90:10 wt%	14 MPa	0.5784	0.2636	0.9714	4.0 ± 1.1
		25 MPa	0.6491	0.3078	0.9945	6.5 ± 2.6
	70:30 wt%	14 MPa	0.5430	0.2665	0.9833	4.4 ± 0.4
		25 MPa	0.6045	0.3196	0.9861	3.5 ± 0.4
SBA-15	90:10 wt%	14 MPa	0.5666	0.1713	0.9437	2.9 ± 0.3
		25 MPa	0.4769	0.2049	0.9756	5.5 ± 1.7
	70:30 wt%	14 MPa	0.6592	0.2833	0.9991	3.6 ± 0.1
		25 MPa	0.6117	0.4834	0.9975	9.4 ± 0.9

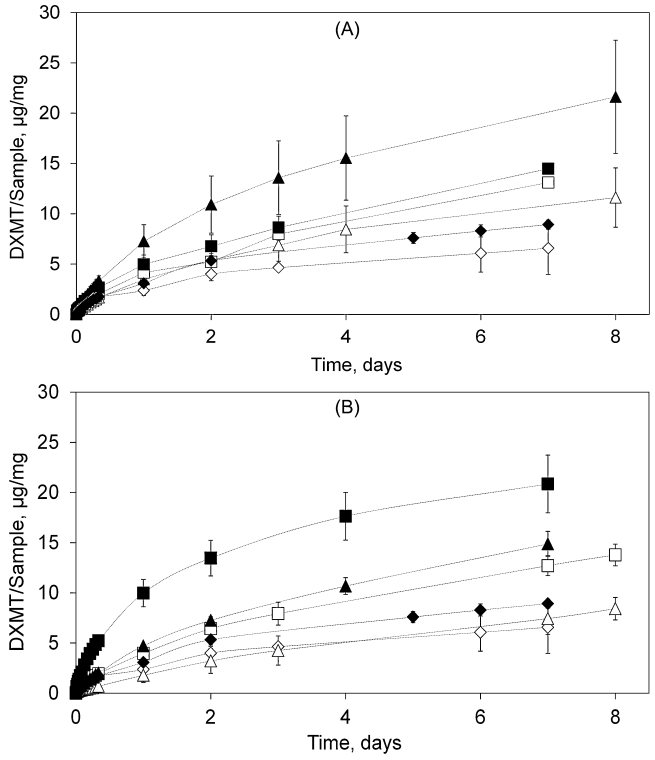

Fig. 9. Release profiles from DXMT-loaded PCL and PCL/SNPs composites. Release results are shown up to an 8 days release period. Samples were processed by $scCO_2$-assisted foaming/mixing (SFM) for 14 h and depressurized at 0.2 dm^3 min^{-1}. Other experimental conditions were: PCL, 14 MPa (◊); PCL, 25 MPa (♦); 90:10 wt%, 14 MPa (△); 90:10 wt%, 25 MPa (▲); 70:30 wt%, 14 MPa (□); and 70:30 wt%, 25 MPa (■). (A) MCM-41 and (B) SBA-15.

4. Conclusions

An environmentally friendly and safe SFM method was implemented to develop PCL/SNPs composite biomaterials presenting adequate chemical, mechanical, morphological and drug loading/release properties that may be helpful for hard tissue engineering applications. SNPs were firstly loaded with DXMT (using a SSID) and later incorporated into PCL + DXMT mixtures (using the SFM method). The SSID method was more efficient than the aqueous soaking to load DXMT into mesoporous SNPs; controlling SSID operational conditions and/or using SNPs with distinct morphological properties enabled tuning the loading yield. Tuning SFM processing conditions (pressure, processing time and depressurization rate) and the MCM-41 relative proportion it was possible to obtain composites with different physicochemical, mechanical and morphological properties (density, porosity, surface area, pore volume, average pore diameter and pore diameter range). Processing of PCL and mesoporous SNPs (MCM-41 and SBA-15) at different proportions and operational conditions rendered distinct DXMT release profiles, with adjustable prolonged release kinetics.

Acknowledgments

This work was supported by FCT-MEC (Portugal), Programa Ciência 2008 (Portugal), FEDER (Portugal, Spain) and COMPETE (Portugal), under contracts PEst-C/EQB/UI0102/2011 and PEst-C/EME/UI0285/2013, MICINN (SAF2011-22771, Spain), Xunta de Galicia (10CSA203013PR; CN2012/045, Spain) and CYTED Red RIMADEL – "Red Iberoamericana de Nuevos Materiales para el Diseño de Sistemas Avanzados de Liberación de Fármacos en Enfermedades de Alto Impacto Socioeconómico". L. Pereiro is acknowledged for helping with the morphological characterization.

Appendix A. Supplementary data

Supplementary data associated with this article can be found, in the online version, at http://dx.doi.org/10.1016/j.ijpharm.2013.08.042.

References

Ahern, R.J., Crean, A.M., Ryan, K.B., 2012. The influence of supercritical carbon dioxide ($SC\text{-}CO_2$) processing conditions on drug loading and physicochemical properties. Int. J. Pharm. 439, 92–99.
Ambrogi, V., Perioli, L., Pagano, C., Marmottini, F., Ricci, M., Sagnella, A., Rossi, C., 2012. Use of SBA-15 for furosemide oral delivery enhancement. Eur. J. Pharm. Sci. 46, 43–48.
Arcos, D., Vallet-Regí, M., 2010. Sol–gel silica-based biomaterials and bone tissue regeneration. Acta Biomater. 6, 2874–2888.
Baker, K.C., Bellair, R., Manitiu, M., Herkowitz, H.N., Kannan, R.M., 2009. Structure and mechanical properties of supercritical carbon dioxide processed porous resorbable polymer constructs. J. Mech. Behav. Biomed. Mater. 2, 620–626.
Banchero, M., Manna, L., 2012. The use of lysine to enhance the supercritical complexation of ketoprofen and cyclodextrins. J. Supercrit. Fluids 67, 76–83.
Belhadj-Ahmed, F., Badens, E., Llewellyn, P., Denoyel, R., Charbi, t G., 2009. Impregnation of vitamin E acetate on silica mesoporous phases using supercritical carbon dioxide. J. Supercrit. Fluids 51, 278–286.
Bose, S., Taradfer, S., 2012. Calcium phosphate ceramic systems in growth factor and drug delivery for bone tissue engineering: a review. Acta Biomater. 8, 1401–1421.
Braga, M.E.M., Costa, V.P., Pereira, M.J.T., Fiadeiro, P.T., Gomes, A.P.A.R., Duarte, C.M.M., de Sousa, H.C., 2011. Effects of operational conditions on the supercritical solvent impregnation of acetazolamide in Balafilcon A commercial contact lenses. Int. J. Pharm. 420, 231–243.
Braga, M.E.M., Pato, M.V., Silva, H.S.R.C., Ferreira, E.I., Gil, M.H., Duarte, C.M.M., de Sousa, H.C., 2008. Supercritical solvent impregnation of ophthalmic drugs on chitosan derivatives. J. Supercrit. Fluids 44, 245–257.
Burg, K.J., Porter, S., Kellam, J.F., 2000. Biomaterial developments for bone tissue engineering. Biomaterials 21, 2347–2359.
Chen, G., Ushida, T., Tateishi, T., 2002. Scaffold design for tissue engineering. Macromol. Biosci. 2, 67–77.
Chim, R.B., de Matos, M.B.C., Braga, M.E.M., Dias, A.M.A., de Sousa, H.C., 2012. Solubility of dexamethasone in supercritical carbon dioxide. J. Chem. Eng. Data 57, 3756–3760.
Chrissafis, K., Antoniadis, G., Paraskevopoulos, K.M., Vassiliou, A., Bikiaris, D.N., 2007. Comparative study of the effect of different nanoparticles on the mechanical properties and thermal degradation mechanism of in situ prepared poly(ε-caprolactone) nanocomposites. Compos. Sci. Technol. 67, 2165–2174.
Collins, N.J., Bridson, R.H., Leeke, G.A., Grover, L.M., 2010. Particle seeding enhances interconnectivity in polymeric scaffolds foamed using supercritical CO_2. Acta Biomater. 6, 1055–1060.
Collins, N.J., Leeke, G.A., Bridson, R.H., Hassan, F., Grover, L.M., 2008. The influence of silica on pore diameter and distribution in PLA scaffolds produced using supercritical CO_2. J. Mater. Sci. Mater. Med. 19, 1497–1502.
Costa, V.P., Braga, M.E.M., Guerra, J.P., Duarte, A.R.C., Duarte, C.M.M., Leite, E.O.B., Gil, M.H.M., de Sousa, H.C., 2010a. Development of therapeutic contact lenses using a supercritical solvent impregnation method. J. Supercrit. Fluids 52, 306–316.
Costa, V.P., Braga, M.E.M., Duarte, C.M.M., Alvarez-Lorenzo, C., Concheiro, A., Gil, M.H., de Sousa, H.C., 2010b. Anti-glaucoma drug-loaded contact lenses prepared using supercritical solvent impregnation. J. Supercrit. Fluids 53, 165–173.
Dash, T.K., Konkimalla, V.B., 2012. Poly-ε-caprolactone based formulations for drug delivery and tissue engineering: a review. J. Control. Release 158, 15–33.
Davies, O.R., Lewis, A.L., Whitaker, M.J., Tai, H., Shakesheff, K.M., Howdle, S.M., 2008. Applications of supercritical CO_2 in the fabrication of polymer systems for drug delivery and tissue engineering. Adv. Drug Deliv. Rev. 60, 373–387.
Dias, A.M.A., Rey-Rico, A., Oliveira, R.A., Marceneiro, S., Alvarez-Lorenzo, C., Concheiro, A., Júnior, R.N.C., Braga, M.E.M., de Sousa, H.C., 2013. Wound dressings loaded with an anti-inflammatory jucá (Libidibia ferrea) extract using supercritical carbon dioxide technology. J. Supercrit. Fluids 74, 34–45.
Dias, A.M.A., Braga, M.E.M., Seabra, I.J., Ferreira, P., Gil, M.H., de Sousa, H.C., 2011. Development of natural-based wound dressings impregnated with bioactive compounds and using supercritical carbon dioxide. Int. J. Pharm. 408, 9–19.
Duarte, A.R.C., Simplício, A.L., Vega-Gonzalez, A., Subra-Paternault, P., Coimbra, P., Gil, M.H., de Sousa, H.C., Duarte, C.M.M., 2007. Supercritical fluid impregnation of a biocompatible polymer for ophthalmic drug delivery. J. Supercrit. Fluids 42, 373–377.
Duarte, A.R.C., Martins, C., Coimbra, P., Gil, M.H.M., de Sousa, H.C., Duarte, C.M.M., 2006. Sorption and diffusion of dense carbon dioxide in a biocompatible polymer. J. Supercrit. Fluids 38, 392–398.
Elvassore, N., Kikic, I., 2001. Pharmaceutical processing with supercritical fluids. In: Bertucco, A., Vetter, G. (Eds.), High Pressure Process Technology: Fundamentals and Applications. Elsevier, Amsterdam, pp. 612–625.

Elzein, T., Nasser-Eddine, M., Delaite, C., Bistac, S., Dumas, P., 2004. FTIR study of polycaprolactone chain organization at interfaces. J. Colloid Interface Sci. 273, 381–387.

Elzubair, A., Elias, C.N., Suarez, J.C.M., Lopes, H.P., Vieira, M.V.B., 2006. The physical characterization of a thermoplastic polymer for endodontic obturation. J. Dentistry 34, 784–789.

Fanovich, M.A., Ivanovic, J., Misic, D., Alvarez, M.V., Jaeger, P., Zizovic, I., Eggers, R., 2013. Development of polycaprolactone scaffold with antibacterial activity by an integrated supercritical extraction and impregnation process. J. Supercrit. Fluids 78, 42–53.

Fanovich, M.A., Jaeger, P., 2012. Sorption and diffusion of compressed carbon dioxide in polycaprolactone for the development of porous scaffolds. Mater. Sci. Eng. C: Mater. Biol. Appl. 32, 961–968.

Fidalgo, A., Ilharco, L.M., 2001. The defect structure of sol–gel-derived silica/polytetrahydrofuran hybrid films by FTIR. J. Non-Cryst. Solids 283, 144–154.

Fleming, O.S., Kazarian, S.C., 2005. Polymer processing with supercritical fluids. In: Kemmere, M.F., Meyer, T. (Eds.), Supercritical Carbon Dioxide in Polymer Reaction Engineering. Wiley-VCH Verlag GmbH & Co., Weinheim, pp. 205–234.

Fruijtier-Pölloth, C., 2012. The toxicological mode of action and the safety of synthetic amorphous silica – a nanostructured material. Toxicology 294, 61–79.

Fu, Q., Saiz, E., Rahaman, M.N., Tomsia, A.P., 2011. Bioactive glass scaffolds for bone tissue engineering: state of the art and future perspectives. Mater. Sci. Eng. C: Mater. Biol. Appl. 31, 1245–1256.

Fukushima, K., Tabuani, D., Camino, G., 2009. Nanocomposites of PLA and PCL based on montmorillonite and sepiolite. Mater. Sci. Eng. C 29, 1433–1441.

Fuller, J.E., Zugates, G.T., Ferreira, L.S., Ow, H.S., Nguyen, N.N., Wiesner, U.B., Langer, R.S., 2008. Intracellular delivery of core–shell fluorescent silica nanoparticles. Biomaterials 29, 1526–1532.

Georgiou, G., Mathieu, L., Pioletti, D.P., Bourban, P.-E., Månson, J.-A.E., Knowles, J.C., Nazhat, S.N., 2007. Polylactic acid-phosphate glass composite foams as scaffolds for bone tissue engineering. J. Biomed. Mater. Res. B: Appl. Biomater. 80, 322–331.

González-Chomón, C., Braga, M.E.M., de Sousa, H.C., Concheiro, A., Alvarez-Lorenzo, C., 2012. Antifouling foldable acrylic IOLs loaded with norfloxacin by aqueous soaking and by supercritical carbon dioxide technology. Eur. J. Pharm. Biopharm. 82, 383–391.

Hansen, E.W., Schmidt, R., Stocker, M., Akporiaye, D., 1995. Self-diffusion coefficient of water confined in mesoporous MCM-41 materials determined by ^{1}H nuclear magnetic resonance spin-echo measurements. Microporous Mater. 5, 143–150.

Harrison, K., 2007. Introduction to polymeric scaffolds for tissue engineering. In: Jenkins, M. (Ed.), Biomedical Polymers. Woodhead Publishing Limited and CRC Press LLC, Cambridge, pp. 1–32.

Higashi, H., Yoshio, I.Y., Arai, Y., 2000. Calculation of self-diffusion and tracer diffusion coefficients near the critical point of carbon dioxide using molecular dynamics simulation. Ind. Eng. Chem. Res. 39, 4567–4570.

Holly, C.E., Schoichet, M.S., Davies, J.E., 2000. Engineering three-dimensional bone tissue in vitro using biodegradable scaffolds: investigating initial cell-seeding density and culture period. J. Biomed. Mater. Res. 51, 376–382.

Howdle, S.M., Watson, M.S., Whitaker, M.J., Popov, V.K., Davies, M.C., Mandel, F.S., Wang, J.D., Shakesheff, K.M., 2001. Supercritical fluid mixing: preparation of thermally sensitive polymer composites containing bioactive materials. Chem. Commun. 1, 109–110.

Jaganathan, H., Godin, B., 2012. Biocompatibility assessment of Si-based nano- and micro-particles. Adv. Drug Deliv. Rev. 64, 1800–1819.

Jenkins, M.J., Harrison, K.L., Silva, M.M.C.G., Whitaker, M.J., Shakesheff, K.M., Howdle, S.M., 2006. Characterisation of microcellular foams produced from semi-crystalline PCL using supercritical carbon dioxide. Eur. Polym. J. 42, 3145–3151.

Jiang, S., Ji, X., An, L., Jiang, B., 2001. Crystallization behavior of PCL in hybrid confined environment. Polymer 42, 3901–3907.

Kaji, H., Sugimoto, T., Kanatani, M., Nishiyama, K., Chihara, K., 1997. Dexamethasone stimulates osteoclast-like cell formation by directly acting on hemopoietic blast cells and enhances osteoclast-like cell formation stimulated by parathyroid hormone and prostaglandin E_2. J. Bone Miner. Res. 12, 734–741.

Kazarian, S.G., 2000. Polymer processing with supercritical fluids. Polymer 42, 78–101.

Kikic, I., Alessi, P., Cortesi, A., Macnaughton, S.J., Foster, N., Spicka, B., 1996. An experimental study of supercritical adsorption equilibria of salicylic acid on activated carbon. Fluid Phase Equilib. 117, 304–311.

Kikic, I., 2009. Polymer-supercritical fluid interactions. J. Supercrit. Fluids 47, 458–465.

Kikic, I., Vecchione, F., 2003. Supercritical impregnation of polymers. Curr. Opin. Solid State Mater. Sci. 7, 399–405.

Kim, C.-H., Cheng, S.-L., Kim, G.S., 1999. Effects of dexamethasone on proliferation, activity, and cytokine secretion of normal human bone marrow stromal cells: possible mechanisms of glucocorticoid-induced bone loss. J. Endocrinol. 162, 371–379.

Kiran, E., 2009. Polymer miscibility, phase separation, morphological modifications and polymorphic transformations in dense fluids. J. Supercrit. Fluids 47, 466–483.

Kiran, E., 2010. Foaming strategies for bioabsorbable polymers in supercritical fluid mixtures. Part I. Miscibility and foaming of poly(l-lactic acid) in carbon dioxide + acetone binary fluid mixtures. J. Supercrit. Fluids 54, 296–307.

Kiran, E., Liu, K., Ramsdell, K., 2008. Morphological changes in poly(ε-caprolactone) in dense carbon dioxide. Polymer 49, 1853–1859.

Kweon, H.Y., Yoo, M.K., KyuPark, I., Kim, T.H., Lee, H.C., Lee, H.-S., Oh, J.-S., Akaike, T., Cho, C.-S., 2003. A novel degradable polycaprolactone networks for tissue engineering. Biomaterials 24, 801–808.

Lee, L.J., Zeng, C., Cao, X., Han, X., Shen, J., Xu, G., 2005. Polymer nanocomposite foams. Compos. Sci. Technol. 65, 2344–2363.

Léonard, A., Calberg, C., Kerckhofs, G., Wevers, M., Jérôme, R., Pirard, J., Germain, A., Blacher, S., 2008. Characterization of the porous structure of biodegradable scaffolds obtained with supercritical CO_2 as foaming agent. J. Porous Mater. 15, 397–403.

Liu, C., Xia, Z., Czernuszk, J.T., 2008. Design and development of three-dimensional scaffolds for tissue engineering. Chem. Eng. Res. Des. 85, 1051–1064.

López-Periago, A., Argemí, A., Andanson, J.M., Fernández, V., García-González, C.A., Kazarian, S.G., Saurina, J., Domingo, C., 2009. Impregnation of a biocompatible polymer aided by supercritical CO_2: evaluation of drug stability and drug–matrix interactions. J. Supercrit. Fluids 48, 56–63.

Masmoudi, Y., Ben, A.L., Forzano, O., Andre, J.-M., Badens, E., 2011. Supercritical impregnation of intraocular lenses. J. Supercrit. Fluids 60, 98–105.

Massman, W.J., 1998. A review of the molecular diffusivities of H_2O, CO_2, CH_4, CO, O_3, SO_2, NH_3, N_2O, NO, and NO_2 in air, O_2 and N_2 near STP. Atmos. Environ. 32, 1111–1127.

Mathieu, L.M., Montjovent, M.-O., Bourban, P.-E., Pioletti, D.P., Månson, J.-A.E., 2005. Bioresorbable composites prepared by supercritical fluid foaming. J. Biomed. Mater. Res. A 75, 89–97.

Messersmith, P.B., Giannelis, E.P., 1995. Synthesis and barrier properties of poly(ε-caprolactone)-layered silicate nanocomposites. J. Polym. Sci. A: Polym. Chem. 33, 1047–1057.

Molinaro, S., Romero, M.C., Boaro, M., Sensidoni, A., Lagazio, C., Morris, M., Kerry, J., 2013. Effect of nanoclay-type and PLA optical purity on the characteristics of PLA-based nanocomposite films. J. Food Eng. 117, 113–123.

Mooney, D.J., Baldwin, D.F., Suh, N.P., Vacanti, J.P., Langer, R., 1996. Novel approach to fabricate porous sponges of poly(D,L-lactic-co-glycolic acid) without the use of organic solvents. Biomaterials 17, 1417–1422.

Morère, J., Tenorio, M.J., Torralvo, M.J., Pando, C., Renuncio, J.A.R., Cabañas, A., 2011. Deposition of Pd into mesoporous silica SBA-15 using supercritical carbon dioxide. J. Supercrit. Fluids 56, 213–222.

National Institute of Standards and Technology (NIST), 2012. http://webbook.nist.gov/chemistry/fluid/ (accessed on 01.02.13).

Natu, M.V., Gil, M.H., de Sousa, H.C., 2008. Supercritical solvent impregnation of poly(ε-caprolactone)/poly (oxyethylene-b-oxypropylene-b-oxyethylene) and poly(ε-caprolactone)/poly(ethylene-vinyl acetate) blends for controlled release applications. J. Supercrit. Fluids 47, 93–102.

Ni, M., Xu, Q.-Q., Yin, J.-Z., 2012. Preparation of controlled release nanodrug ibuprofen supported on mesoporous silica using supercritical carbon dioxide. J. Mater. Res. 27, 2902–2910.

Ogoshi, T., Chujo, Y., 2005. Organic–inorganic polymer hybrids prepared by the sol–gel method. Compos. Interfaces 11, 539–566.

Pitha, J., Milecki, J., Fales, H., Panell, L., Uekama, K., 1986. Hydroxypropyl-β-cyclodextrin: preparation and characterization; effects on solubility of drugs. Int. J. Pharm. 29, 73–82.

Prakash, S.S., Brinker, C.J., Hurd, A.J., 1995. Silica aerogel films at ambient pressure. J. Non-Cryst. Solids 190, 264–275.

Rahman, M.N., Day, D.E., Sonny, B., Fu, Q., Jung, S.B., Bonewald, L.F., Tomsia, A.P., 2011. Bioactive glass in tissue engineering. Acta Biomater. 7, 2355–2373.

Reverchon, E., Cardea, S., 2012. Supercritical fluids in 3-D tissue engineering. J. Supercrit. Fluids 69, 97–107.

Rosenholm, J.M., Peuhu, E., Bate-Eya, L.T., Eriksson, J.E., Sahlgren, C., Lindén, M., 2010. Cancer-cell-specific induction of apoptosis using mesoporous silica nanoparticles as drug-delivery vectors. Small 6, 1234–1241.

Rouholamin, D., Smith, P.J., Ghassemieh, E., 2013. Control of morphological properties of porous biodegradable scaffolds processed by supercritical CO_2 foaming. J. Mater. Sci. 48, 3254–3263.

Sachlos, E., Czernuszka, J.T., 2003. Making tissue engineering scaffolds work. Review: the application of solid freeform fabrication technology to the production of tissue engineering scaffolds. Eur. Cell Mater. 5, 29–40.

Salerno, A., Di Maio, E., Iannace, S., Netti, P.A., 2011. Solid-state supercritical CO_2 foaming of PCL and PCL-HA nano-composite: effect of composition, thermal history and foaming process on foam pore structure. J. Supercrit. Fluids 58, 158–167.

Salgado, A.J., Coutinho, O.P., Reis, R.L., 2004. Bone tissue engineering: state of the art and future trends. Macromol. Biosci. 4, 743–765.

Sanchez, C., Belleville, P., Popall, M., Nicole, L., 2011. Applications of advanced hybrid organic-inorganic nanomaterials: from laboratory to market. Chem. Soc. Rev. 40, 696–753.

Schantz, J.-T., Hutmacher, D.W., Lam, C.X.F., Brinkmann, M., Wong, K.M., Lim, T.C., Chou, N., Guldberg, R.E., Teoh, S.H., 2004. Repair of calvarial defects with customized tissue-engineered bone grafts I. Evaluation of osteogenesis in a three-dimensional culture system. Tissue Eng. 9, 127–139.

Shieh, Y.-T., Lai, J.-G., Tang, W.-L., Yang, C.-H., Wang, T.-L., 2009. Supercritical CO_2 intercalation of polycaprolactone in layered silicates. J. Supercrit. Fluids 49, 385–393.

Shieh, Y.-T., Yang, H.-S., 2005. Morphological changes of polycaprolactone with high-pressure CO_2 treatment. J. Supercrit. Fluids 33, 183–192.

Siepmann, J., Peppas, N.A., 2001. Modeling of drug release from delivery systems based on hydroxypropyl methylellulose (HPMC). Adv. Drug Deliv. Rev. 48, 139–157.

Siepmann, J., Siepmann, F., 2011. Modeling of diffusion controlled drug delivery. J. Control. Release 161, 351–362.
Subramaniam, B., Rajewski, R.J., Snavely, K., 1997. Pharmaceutical processing with supercritical carbon dioxide. J. Pharm. Sci. 86, 885–890.
Tabata, Y., 2005. Significance of release technology in tissue engineering. Drug Discovery Today 10, 1639–1646.
Tai, H., Popov, V.K., Shakesheff, K.M., Howdle, S.M.a., 2007a. Putting the fizz into chemistry: applications of supercritical carbon dioxide in tissue engineering, drug delivery and synthesis of novel block copolymers. Biochem. Soc. Trans. 35, 516–521.
Tai, H., Mather, M.L., Howard, D., Wang, W., White, L.J., Crowe, J.A., Morgan, S.P., Chandra, A., Williams, D.J., Howdle, S.M., Shakesheff, K.M.b., 2007b. Control of pore size and structure of tissue engineering scaffolds produced by supercritical fluids processing. Eur. Cells Mater. 14, 64–77.
Teng, X., Ren, J., Gu, S., 2007. Preparation and characterization of porous PDLLA/HA composite foams by supercritical carbon dioxide technology. J. Biomed. Mater. Res. B: Appl. Biomater. 81B, 185–193.
Tsimpliaraki, A., Tsivintzelis, I., Marras, S.I., Zuburtikudis, I., Panayiotou, C., 2011. The effect of surface chemistry and nanoclay loading on the microcellular structure of porous poly(d,l lactic acid) nanocomposites. J. Supercrit. Fluids 57, 278–287.
Tsivintzelis, I., Angelopoulou, A.G., Panayiotou, C., 2007. Foaming of polymers with supercritical CO_2: an experimental and theoretical study. Polymer 48, 5928–5939.
Vallet-Regí, M., Balas, F., Arcos, D., 2007. Mesoporous materials for drug delivery. Angew. Chem. Int. Ed. 46, 7548–7558.
Vallet-Regí, M., Colilla, M., González, B., 2011a. Medical applications of organic-inorganic hybrid materials within the field of silica-based bioceramics. Chem. Soc. Rev. 40, 596–607.
Vallet-Regí, M., Hernández Ruis, E., 2011b. Bioceramics: from bone regeneration to cancer nanomedicine. Adv. Mater. 23, 5177–5218.
Vivero-Escoto, J.L., Slowing, I.I., Trewyn, B.G., Lin, VS-Y, 2010. Mesoporous silica nanoparticles for intracellular controlled drug delivery. Small 6, 1952–1967.
Williams, J.J., Wiersum, A.D., Seaton, N.A., Düren, T., 2011. Influence of surface groups on the diffusion of gases in MCM-41: a molecular dynamics study. J. Phys. Chem. C 115, 10651–10660.
Xu, Q., Ren, X., Chang, Y., Wang, J., Yu, L., Dean, K., 2004. Generation of microcellular biodegradable polycaprolactone foams in supercritical carbon dioxide. J. Appl. Polym. Sci. 94, 593–597.
Yalkowsky, S.H., He, Y. (Eds.), 2003. Handbook of Aqueous Solubility Data. CRC Press LLC, New York, p. 1197.
Yañez, F., Martikainen, L., Braga, M.E.M., Alvarez-Lorenzo, C., Concheiro, A., Duarte, C.M.M., Gil, M.H., de Sousa, H.C., 2011. Supercritical fluid-assisted preparation of imprinted contact lenses for drug delivery. Acta Biomater. 7, 1019–1030.
Zhai, W., Yu, J., Wum, L., Ma, W., He, J., 2006. Heterogeneous nucleation uniformizing cell size distribution in microcellular nanocomposites foams. Polymer 47, 7580–7589.